JCTC Journal of Chemical Theory and Computation

Fully Numerical All-Electron Solutions of the Optimized Effective Potential Equation for Diatomic Molecules

Adi Makmal,[†] Stephan Kümmel,[‡] and Leeor Kronik*,[†]

Department of Materials and Interfaces, Weizmann Institute of Science, Rehovoth 76100, Israel, and Physikalisches Institut, Universität Bayreuth, D-95440 Bayreuth, Germany

Received November 10, 2008

Abstract: We present an approach for fully numerical, all-electron solutions of the optimized effective potential equation within Kohn−Sham density functional theory for diatomic molecules. The approach is based on a real-space, prolate-spheroidal coordinate grid for solving the all-electron Kohn−Sham equations and an iterative scheme for solving the optimized effective potential equation. The accuracy of this method is demonstrated by comparison with previously reported calculations. New fully numerical benchmark results for selected diatomic molecules are provided.

1. Introduction

The Kohn−Sham formulation of density functional theory (DFT)[1−3] is a widely used approach for calculating the electronic structure of materials from first principles. In Kohn−Sham DFT, the original interacting-electron Schrödinger equation is mapped into an equivalent noninteracting problem. This leads to effective one-particle equations which, in the spin-polarized form[4] are

$$\left(-\frac{\nabla^2}{2} + V_{\text{ion}}(\mathbf{r}) + V_{\text{H}}(\mathbf{r}) + V_{\text{xc},\sigma}(\mathbf{r})\right)\varphi_{i\sigma}(\mathbf{r}) = \varepsilon_{i\sigma}\varphi_{i\sigma}(\mathbf{r}) \tag{1}$$

where σ is a spin index, $\varphi_{i\sigma}$ and $\varepsilon_{i\sigma}$ are the ith Kohn−Sham orbital and energy, respectively, V_{ion} is the ion−electron attraction potential, V_{H} is the Hartree potential, and $V_{\text{xc},\sigma}$ is the exchange-correlation potential that represents all nonclassical electron interactions (hartree atomic units are used throughout unless otherwise stated). The exchange-correlation potential is the functional derivative of the exchange-correlation energy (which is a functional of the charge density) with respect to the (spin-polarized) charge density, $\rho_\sigma(\mathbf{r})$

$$V_{\text{xc},\sigma}(\mathbf{r}) \equiv \frac{\delta}{\delta\rho_\sigma(\mathbf{r})}E_{\text{xc}}[\rho_\uparrow(\mathbf{r}), \rho_\downarrow(\mathbf{r})] \tag{2}$$

Although DFT is exact in principle, the exact form of $E_{\text{xc}}[\rho_\uparrow(\mathbf{r}),\rho_\downarrow(\mathbf{r})]$ is unknown, and in practice approximate forms must be used.

Orbital-dependent functionals are exchange-correlation functionals that use Kohn−Sham orbitals, themselves being functionals of the density, as ingredients in functional construction. Such functionals are currently considered to be one of the most promising avenues in modern DFT, as they hold the promise of overcoming some of the more serious deficiencies of exchange-correlation functionals that are explicit functionals of the density.[5] A major difficulty, however, with implicit density functionals for the exchange-correlation energy is that a direct derivative for determining the exchange-correlation potential is not available. Instead, chain-rule arguments lead to an integro−differential equation, generally known as the optimized effective potential (OEP) equation.[5−12] There are several equivalent formulations for the OEP equation; here we use the (relatively) simple form[11,13,14]

$$S_\sigma(\mathbf{r}) \equiv \sum_{i=1}^{N_\sigma} \psi^*_{i\sigma}(\mathbf{r})\varphi_{i\sigma}(\mathbf{r}) + c.c. = 0 \tag{3}$$

where N_σ is the number of occupied states in the σ spin channel. Here $\psi^*_{i\sigma}(\mathbf{r})$ are called "orbital shifts" and are given by

* Corresponding author phone: +972-8-934-4993; e-mail: leeor.kronik@weizmann.ac.il.

[†] Weizmann Institute of Science.

[‡] Universität Bayreuth.

10.1021/ct800485v CCC: $40.75
Published on Web 06/11/2009

$$\psi^*_{i\sigma}(\mathbf{r}) = -\sum_{j\neq i}^{\infty} \frac{\int \varphi^*_{i\sigma}(\mathbf{r}')[u^{\mathrm{xc}}_{i\sigma}(\mathbf{r}') - V^{\mathrm{OEP}}_{\mathrm{xc},\sigma}(\mathbf{r}')]\varphi_{j\sigma}(\mathbf{r}')\,\mathrm{d}^3r'}{\varepsilon_{i\sigma} - \varepsilon_{j\sigma}}\varphi^*_{j\sigma}(\mathbf{r}), \quad \varepsilon_{i\sigma} \neq \varepsilon_{j\sigma} \tag{4}$$

where

$$u^{\mathrm{xc}}_{i\sigma}(\mathbf{r}) = \frac{1}{\varphi^*_{i\sigma}(\mathbf{r})}\frac{\delta E_{\mathrm{xc}}[\{\varphi\}]}{\delta\varphi_{i\sigma}(\mathbf{r})} \tag{5}$$

Because of the complexity of the OEP equation, many approximate schemes for determining $V^{\mathrm{OEP}}_{\mathrm{xc},\sigma}(\mathbf{r})$ have been suggested.[5] Some of them, e.g., the Krieger, Li, and Iafrate (KLI) approximation,[15] or the common energy denominator approximation (CEDA)[16] (which is equivalent to the localized Hartree−Fock (LHF) approach),[17] often provide an excellent approximation to the correct solution of the OEP equation. Nevertheless, it has been shown that, for various properties, use of potentials other than the full OEP may lead to results that are significantly different quantitatively[18−21] or even qualitatively[22,23] from the full OEP solution. This clearly establishes the need for accurate solutions of the OEP equation.

Typically, the Kohn−Sham equations are solved either by employing pseudopotentials (usually in conjunction with a plane-wave basis or a real-space grid), or by using atomic basis sets. Unfortunately, the use of either approach together with the OEP equation raises new difficulties and controversies:[5] OEP-compatible pseudopotentials require special care in their construction if spurious "potential tails" are to be avoided,[24−27] and even then questions as to the importance of core−valence interaction may be raised.[28] Use of localized basis sets may result in numerical inaccuracies[29] and an ill-defined algebraic problem, an issue whose resolution has recently attracted much discussion.[5,30−36]

In light of the above difficulties, it is highly desirable to obtain benchmark OEP calculations, i.e., "fully numerical" ones, where the only approximation beyond unavoidable roundoff errors is the choice of the exchange-correlation functional. Such calculations could be used for development and testing of new orbital-dependent functionals, as well as for objective testing of various approximate OEP solution schemes. To the best of our knowledge, prior to the present work this was achieved only for single atoms,[7,11,14,37,38] an unsatisfactory state of affairs because chemical bonds cannot be examined. Here, we present a real-space, prolate-spheroidal coordinate[39] based approach for fully numerical, all-electron solutions of the OEP equation for diatomic molecules. In the following, we explain the prolate-spheroidal real-space grid and the main principles of the numerical approach. We then demonstrate the accuracy of the proposed scheme via both OEP and non-OEP calculations for several chemical systems and functionals.

2. Numerical Approach

Following Becke,[39] Laaksonen and co-workers,[40,41] Grabo et al.,[10] and Engel et al.[42,43] we use a real-space grid based on prolate-spheroidal coordinates. These coordinates are useful for describing a system with two atomic centers

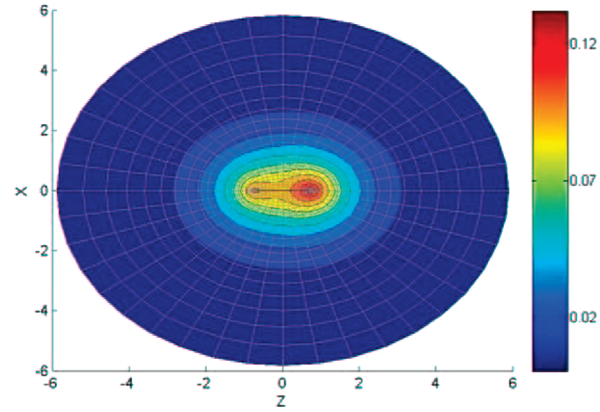

Figure 1. Contour plot of a hypothetical charge density of a heteronuclear dimer, sampled on a prolate-spheroidal coordinate grid. Here, the distance between the two centers is $R = 1.5$ and grid parameters are $N_\mu = 22$, $N_\nu = 20$, and $\mu_{\max} = 2.75$. For clarity, both $\phi = 0$ and $\phi = \pi$ planes are shown, corresponding to positive and negative x values, respectively. During calculation only the plane $\phi = 0$ is explicitly considered.

because the grid is very dense near the two centers, but increasingly coarse with increasing distance from the centers. This property of the grid is most helpful for all-electron calculations because it allows better sampling near the atoms where the ionic potential is singular and the orbitals oscillate rapidly.

For two centers at $A(x = 0, y = 0, z = -R/2)$ and $B(x = 0, y = 0, z = R/2)$, the prolate-spheroidal coordinates $(\mu, \nu, \phi) \in [0, \infty] \times [0, \pi] \times [0, 2\pi]$ are defined by

$$\begin{aligned} x &= \frac{R}{2}\sinh(\mu)\sin(\nu)\cos(\phi), \\ y &= \frac{R}{2}\sinh(\mu)\sin(\nu)\sin(\phi), \\ z &= \frac{R}{2}\cosh(\mu)\cos(\nu) \end{aligned} \tag{6}$$

The geometrical meaning of eq 6 is apparent from the inverse transformation

$$\mu = \cosh^{-1}\left(\frac{r_A + r_B}{R}\right), \quad \nu = \cos^{-1}\left(\frac{r_A - r_B}{R}\right), \quad \phi = \tan^{-1}\left(\frac{y}{x}\right) \tag{7}$$

where $r_A(\mathbf{r})$ and $r_B(\mathbf{r})$ are the Euclidean distances of a general point (x, y, z) from the centers A and B, respectively, and ϕ is the angle of rotation around the interatomic axis, i.e., the z-axis. At any constant-ϕ plane, constant-μ and constant-ν lines correspond to (half) ellipses and hyperbolas, respectively, as shown in Figure 1 for both $\phi = 0$ and $\phi = \pi$.

Due to the cylindrical symmetry of diatomic molecules, the angle ϕ can be treated analytically, and the problem is effectively reduced to a two-dimensional one. Formally, this means that all physical entities (e.g., charge density, potentials, squared absolute wave functions, etc.) are ϕ-independent and that the one-particle wave functions are of the form

$$\varphi(\mu, \nu, \phi) = \varphi(\mu, \nu, 0)\mathrm{e}^{\mathrm{i}m\phi} \qquad m = 0, \ \pm 1, \ \pm 2, \ldots \tag{8}$$

where m is an integer corresponding to the quantum number of angular momentum with respect to the interatomic axis.

Our numerical approach is based on self-consistent solutions of the Kohn−Sham and OEP equations on the uniform, two-dimensional (μ, ν) grid, using the high-order finite difference approach,[44,45] in which several neighbors around each point are used for approximating derivatives. In the context of pseudopotential-based calculations, the high-order finite difference approach has evolved into a powerful software suite, known as PARSEC (pseudopotential algorithm for real-space electronic structure calculations),[46−48] which has found many successful applications to large-scale electronic structure studies in general[48] and to OEP solutions in particular.[20,22,23] This offers a natural starting point for the present numerical approach, which we implemented in a related yet independent code we call DARSEC (diatomic all-electron real-space electronic structure calculations). Because the high-order finite difference approach in general has been discussed in detail elsewhere, here we naturally focus on aspects that are unique to the prolate-spheroidal grid and/or to the solution of the OEP equation.

The main issue that requires careful attention on a two-dimensional prolate-spheroidal grid is the evaluation of the Laplacian operator. Analytically, after elimination of the ϕ coordinate using eq 8, the Laplacian takes the form

$$\Delta_m(\mu,\nu) = \frac{4}{R^2(\xi^2-\eta^2)}\left[\frac{\partial^2}{\partial\mu^2} + \frac{\xi}{\sqrt{\xi^2-1}}\frac{\partial}{\partial\mu} + \frac{\partial^2}{\partial\nu^2} + \frac{\eta}{\sqrt{1-\eta^2}}\frac{\partial}{\partial\nu} - m^2\left(\frac{1}{\xi^2-1} + \frac{1}{1-\eta^2}\right)\right] \quad (9)$$

where $\xi = \cosh(\mu)$ and $\eta = \cos(\nu)$. One complication is that eq 9 implies that a different Laplacian, Δ_m, and ergo a different Hamiltonian, H_m, is to be operated on functions with different $|m|$ values. Fortunately, this is not a prohibitive complication in practice. According to eq 9 the Kohn−Sham Hamiltonian, H_m, is given by

$$H_m = H_0 + m^2 f(\mu,\nu),$$
$$f(\mu,\nu) = \frac{2}{R^2(\cosh^2(\mu)-\cos^2(\nu))}\times \left(\frac{1}{\cosh^2(\mu)-1} + \frac{1}{1-\cos^2(\nu)}\right) > 0 \quad \forall\mu \geq 0, \quad \pi \geq \nu \geq 0 \quad (10)$$

Denoting the lowest energy eigenvalue and orbital, per a given m, by ε°_m and φ°_m, respectively, we obtain from eq 10 and the variational principle that for $|\tilde{m}| > |m|$

$$\varepsilon^\circ_{\tilde{m}} = \langle\varphi^\circ_{\tilde{m}}|H_{\tilde{m}}|\varphi^\circ_{\tilde{m}}\rangle > \langle\varphi^\circ_{\tilde{m}}|H_m|\varphi^\circ_{\tilde{m}}\rangle \geq \min_\varphi\langle\varphi|H_m|\varphi\rangle = \langle\varphi^\circ_m|H_m|\varphi^\circ_m\rangle = \varepsilon^\circ_m \quad (11)$$

Equation 11 shows that the lowest eigenvalue of H_m is lower than the lowest eigenvalue of $H_{\tilde{m}}$. This means that even though there are an infinite number of $|m|$ values, it suffices to consider a finite (and typically small) set of them, starting from $m = 0$ and onward, in order to compute all the filled states with no risk of missing any such states. In each self-consistent cycle, all relevant Hamiltonians H_m are diagonalized and the density constructed from the solutions of all of them is used to update the Hamiltonians.

A second complication associated with the Laplacian of eq 9 is that it is singular along the $\mu = 0$ and $\nu = 0$, π boundaries of the (μ, ν) domain, which together make up the interatomic axis in real space. This can be handled in two ways. One approach, employed by Kobus et al.,[41] is that orbital values on this axis are to be interpolated. In fact such interpolation is necessary only for $m = 0$, because for all $|m| > 0$ all orbitals vanish identically on the interatomic axis. Alternatively, one can shift the grid by half a grid spacing in both the μ and the ν directions, such that no grid points are found on the singular line. We implemented both approaches and did not observe pronounced differences in performance between them.

The third complication associated with the Laplacian of eq 9 is that it is not Hermitian (see also Becke).[39] This makes the employment of algorithms that assume Hermiticity problematic. There are several ways to mitigate this problem considerably and a detailed discussion is provided in Appendix A.

We now briefly review the calculation of the various potential terms in the Kohn−Sham eq 1. The ionic potential is simply taken as the exact one, i.e.,

$$V_{\text{ion}}(\mathbf{r}) = -\frac{Z_A}{r_A(\mathbf{r})} - \frac{Z_B}{r_B(\mathbf{r})} \quad (12)$$

where Z_A and Z_B are the atomic numbers of atoms A and B, respectively, and with $r_A(\mathbf{r})$ and $r_B(\mathbf{r})$ defined after eq 7. Solutions of a single atom are also possible, by setting Z_A (or Z_B) to zero. The Hartree potential, $V_{\text{H}}(\mathbf{r})$, is obtained from a solution of the Poisson equation $\Delta_m V_{\text{H}}(\mathbf{r}) = -4\pi\rho(\mathbf{r})$ (with $m = 0$ due to the cylindrical symmetry of $V_{\text{H}}(\mathbf{r})$) using the conjugate gradient method.[49] Because the grid is typically quite small, boundary conditions are evaluated using direct integration. As for the exchange-correlation potential, in exact-exchange calculations the terms $P_{ij}(\mathbf{r}) = \int(\varphi^*_{i\sigma}(\mathbf{r}')\varphi_{j\sigma}(\mathbf{r}'))/(|\mathbf{r}-\mathbf{r}'|)\,d^3r'$ are needed for constructing $u^{\text{xc}}_{i\sigma}(\mathbf{r})$ of eq 5. They are evaluated by solving Poisson-like equations, with $\rho_{ij}(\mathbf{r}) = \varphi^*_{i\sigma}(\mathbf{r})\varphi_{j\sigma}(\mathbf{r})$ on the right-hand side instead of $\rho(\mathbf{r})$, using the same method. In this case a value of $m = |m_i - m_j|$ has to be used for applying the Laplacian Δ_m. Finally, the OEP equation is solved using the "S-iteration" method.[14,50] Briefly, the exchange-correlation potential is updated iteratively according to

$$V^{\text{OEP}}_{\text{xc},\sigma_{\text{new}}}(\mathbf{r}) = V^{\text{OEP}}_{\text{xc},\sigma_{\text{old}}}(\mathbf{r}) + cS_\sigma(\mathbf{r}) \quad (13)$$

with $S_\sigma(\mathbf{r})$ defined in eq 3 and where c is a real positive parameter that is manually adjusted for optimal convergence. Details regarding the calculation of the orbital shifts defined in eq 4, that are needed to evaluate $S_\sigma(\mathbf{r})$, are given in Appendix B.

Because all potentials are strictly local, they only provide diagonal entries on the (μ, ν) Hamiltonian matrix. Hence, just like in PARSEC, the Hamiltonian is extremely sparse. Here, off-diagonal elements, and very few of them at that, are introduced only by the matrix representation of the Laplacian (the Hamiltonian here is even sparser than that of

PARSEC due to the absence of a nonlocal pseudopotential term). The full Hamiltonian matrix is therefore never computed nor stored. Instead, the operation of the Hamiltonian matrix on an orbital is evaluated by explicitly considering only its diagonal values and the high-order finite difference expansion coefficients, which is very efficient computationally.

A different issue which we found to be of importance is the numerical evaluation of the various integrals arising in the computation. We used the high-order integration scheme recommended by Kobus et al.,[41] which is based on the seven-point Newton−Cotes integration formula, i.e.,

$$\int_{x_1}^{x_7} f(x)\,\mathrm{d}x \cong \sum_{i=1}^{7} c_i f_i h \qquad \text{with} \qquad c_1 = c_7 = \frac{41}{140},$$
$$c_2 = c_6 = \frac{216}{140}, \quad c_3 = c_5 = \frac{27}{140}, \quad c_4 = \frac{272}{140} \quad (14)$$

This integration scheme facilitates convergence with grids that are significantly sparser than those needed using simple summation and allows for huge savings in both computer time and memory. Specifically, we used the expression:

$$\int f(\mu,\nu)\,\mathrm{d}^3 r = \int_0^{2\pi}\mathrm{d}\phi \int_0^{\infty}\mathrm{d}\mu \int_0^{\pi}\mathrm{d}\nu\, \mathscr{J}(\mu,\nu) f(\mu,\nu)$$
$$\cong 2\pi \sum_{i=1}^{N_\mu}\sum_{j=1}^{N_\nu} \tilde{c}_i \tilde{c}_j \mathscr{J}(\mu_i,\nu_j) f(\mu_i,\nu_j) h_\mu h_\nu \quad (15)$$

where $\mathscr{J}(\mu, \nu, \phi)$ is the volume element, given by

$$\mathscr{J}(\mu,\nu,\phi) = \left(\frac{R}{2}\right)^3 (\cosh^2(\mu) - \cos^2(\nu)) \sinh(\mu) \sin(\nu) \quad (16)$$

and $\tilde{c}_i$ are based on the Newton−Cotes coefficients c_i of eq 14.[51] Obviously this means that the number of grid points in the μ and ν directions must be of the form of $6n + 1$, where n is an integer.

We conclude this section with some practical comments on the DARSEC code in which the above concepts are implemented. Like PARSEC, DARSEC is a modern, massively parallel (using the message passing interface protocol) Fortran 90/95 code. Currently, DARSEC uses the ARPACK software package[52] to diagonalize the Kohn−Sham Hamiltonians, but the approach is generic, and other solvers can easily be used (because the Laplacian matrix is real but not symmetic, we use the nonsymmetric, real ARPACK solver). Similarly, below we provide examples based on local density approximation (LDA) and exact-exchange, but the code is designed such that any orbital-dependent functional can be combined with OEP in a straightforward manner. For the systems considered below, DARSEC requires a few minutes to several hours and a modest few hundreds MB of memory for a complete LDA or exchange-only KLI solution with an accuracy of 10^{-5} hartree in total energies and eigenvalues.

As expected, in non-OEP calculations the majority of the computation time is devoted to the iterative diagonalization process. Our empirical experience with ARPACK shows that using a relatively large amount of Arnoldi basis vectors (of the order of thousands) usually decreases the run time dramatically (by up to 2 orders of magnitudes). We attribute this primarily to the above-discussed singularity of the Laplacian operator along the interatomic axis. A numerical convergence of the order of 10^{-5} hartree is usually achieved by less than 15 self-consistent iterations. This number can be reduced significantly, typically to less than five iterations, by using interpolated converged results from a sparser grid as a starting point for the denser one. For OEP calculations, the required run time for achieving comparable accuracies increases, possibly up to several days, for two main reasons: (a) OEP calculations are typically slower to converge and may require tens of self-consistent iterations; (b) the orbital shifts do not always converge smoothly, and different starting vectors for the conjugate gradient computation of the orbital shifts (see Appendix B) may be needed.

Table 1. Total Energy, in hartree, for the CO Molecule, Calculated with Grids of Increasing Density and Size[a]

	CO−xKLI			
$\{N_\mu, N_\nu\}$	μ_{max}	total energy	ΔE	N_A
{61, 43}	3.86	−112.78377		1300
{85, 55}	3.87	−112.78315	0.00062	1300
{109, 73}	3.98	−112.78320	−0.00005	1600
{133, 103}	4.18	−112.783222	−0.00002	1800
{151, 121}	4.39	−112.783223	−0.000001	2300
Engel et al.[b]		−112.78340		

[a] N_μ, N_ν, number of grid points along the μ, ν directions, respectively; μ_{max}, maximum value of μ used in calculation; ΔE, difference between current total energy and the total energy obtained by the previous coarser grid, in hartree; N_A, number of Arnoldi basis vectors used during diagonalization. [b] For comparison the xKLI total energy of CO as calculated by Engel et al. (ref 43) using a similar prolate-spheroidal coordinate grid and bond length of 2.1316 au is also provided.

In Table 1 we provide convergence details for the representative case of the CO molecule with the experimental equilibrium bond length of 2.132 au,[53] studied using the KLI approximation to the exact-exchange functional. We focus on the convergence of the total energy with respect to the sparsity of the grid (number of grid points) and its size (determined by μ_{max}). Clearly convergence to 10^{-5} hartree was achieved for the largest grid (for which the run time was of the order of several hours), and convergence to 10^{-3} hartree was achieved for a very modest grid indeed. It is our general experience, for this and other systems, that the convergence rate of OEP calculations with increasing grid size is similar.

3. Results

In this section we present detailed numerical results obtained using the above-explained approach. Calculations were performed with the LDA[54,55] or with exact-exchange (and no correlation). For the latter functional, the exchange-potential was given either by the KLI approximation (xKLI) or by a full OEP calculation (xOEP). First, we reproduce known results so as to verify our methodology. Then, we provide new fully numerical exact-exchange OEP results for selected diatomic molecules. All calculations were converged to at least 10^{-4} hartree in the total energy (note that the eigenvalues may exhibit larger errors),

Table 2. Numerical Parameters Used in This Work[a]

system	R_{AB} [au]	N_μ	N_ν	μ_{max} (r_{sa} [au])	S	c
			xcLDA:			
H_2	1.446	85	85	4.22 (24.71)		
BH	2.373	85	85	4.32 (44.79)		
Li_2	5.120	85	85	4.32 (96.65)		
			xKLI and xOEP:			
H	0.5	37	25	6.37 (73.31)	1	1.0
H_2^+	2.0	31	31	5.39 (109.35)	1	1.0
He	0.5	61	61	4.43 (28.68)	1	5.0
Li	0.5	61	61	5.43 (28.68)	100	3.0
Be	0.5	73	55	5.16 (21.87)	200	3.5
LiH	3.015	109	91	3.82 (34.38)	100	7.2
BH	2.336	79	79	4.15 (37.00)	200	5.5
Li_2	5.051	109	91	3.44 (39.37)	200	6.5
CO	2.132	109	73	3.98 (28.56)	100	0.7

[a] R_{AB}, interatomic distance; N_μ, N_ν, number of grid points along the μ, ν directions; μ_{max}, maximum value of μ; r_{sa}, length of the semiminor axis; S (OEP calculations only), number of S-iterations used during the convergence process; c (OEP calculations only), typical value of convergence parameter used in the S-iterations, see eq 13.

Table 3. Ground-State Total Energies and HOMO Eigenvalues, in hartree, for H_2, BH, and Li_2, Calculated with LDA

	total energy [hartree]		HOMO [hartree]	
LDA	Grabo et al.[a]	DARSEC	Grabo et al.[a]	DARSEC
H_2	−1.137692	−1.137692(1)	−0.373092	−0.3730920(7)
BH	−24.9770	−24.97695(2)	−0.2041	−0.2040(7)
Li_2	−14.7245	−14.7244(5)	−0.1187	−0.1186(6)

[a] Ref 10.

with the first unconverged digit placed in parentheses. Numerical parameters for all calculations presented below are given in Table 2.

For verifying our solutions to the Kohn−Sham equation, we calculated the electronic structures of H_2, BH, and Li_2 using the LDA. The resulting total energies and highest occupied molecular orbital (HOMO) energies are given in Table 3 and are compared to the all-electron calculations of Grabo et al.,[10] performed on a similar prolate-spheroidal grid. All diatomic calculations were performed using the same bond lengths as used by Grabo et al.[10] The comparison immediately confirms that the results do indeed agree to within the stated accuracy of 0.1 mhartree.

As a first step toward verifying our all-electron xKLI and xOEP, we performed calculations for the one-electron systems of H and H_2^+, for which xKLI and xOEP are identical and should yield the exact results. Indeed we found that the two solutions always agreed on all converged digits. Table 4 compares DARSEC calculations for the first 14 energy levels ($n = 1-3$) of a single H atom with the analytical values, demonstrating excellent accuracy. Table 5 shows a similar comparison, for H_2^+, of DARSEC values with analytical values[56,57] and with numerical Hartree−Fock (HF) values (also exact for single-electron systems),[58] at the equilibrium bond length of 2.0 au. Note that the "analytical" values are not always correct to the last digit reported, because of numerical approximations used in the algebraic solutions,[56] whereas the results of Laaksonen et al.[58] were shown to be correct to at least the ninth digit, via comparison

Table 4. Ground-State Total Energy and Energy Levels, in rydbergs, for the H Atom, Calculated with xKLI and xOEP

H	exact	DARSEC (xKLI, xOEP)	m
E_{tot}	−1	−1.00000000(3)	
1s	−1	−1.00000000(8)	0
2s	−1/4	−0.25000000(6)	0
2p	−1/4	−0.25000000(6)	−1, 0, 1
3s	−1/9	−0.1111111(2)	0
3p	−1/9	−0.11111111(8)	−1, 0, 1
3d	−1/9	−0.11111111(5)	−2, −1, 0, 1, 2

Table 5. Ground-State Total Energy and Energy Levels, in hartree, for H_2^+, at the Equilibrium Bond Length of 2.0 au, Calculated with xKLI and xOEP

H_2^+	analytical results[a]	Hartree−Fock[b]	DARSEC (xKLI, xOEP)
E_{tot}	−0.6026[c]	−0.6026342145[d]	−0.6026342144(7)
$1\sigma_g(1s)$	−1.102625	−1.102634214497	−1.1026342144(7)
$1\sigma_u(2p)$	−0.667535	−0.667534392205	−0.667534392(1)
$1\pi_u(2p)$	−0.428775	−0.428771819894	−0.428771819(9)
$2\sigma_g(2s)$	−0.360865	−0.36086487543	−0.3608648754(0)
$2\sigma_u(3p)$	−0.255415	−0.25541316515	−0.2554131651(7)
$3\sigma_g(3d)$	−0.235775	−0.235777628822	−0.2357776288(4)
$1\pi_g(3d)$	−0.226700	−0.22669962663	−0.2266996266(7)
$1\delta_g(3d)$		−0.21273268176	−0.212732681(8)
$2\pi_u(3p)$		−0.20086482987	−0.200864830(1)
$4\sigma_g$	−0.177680		−0.177681045(7)
$3\sigma_u$	−0.137315		−0.13731292(5)
$5\sigma_g$			−0.130791877(9)
$2\pi_g(4d)$		−0.12671013060	−0.12671013(1)
$4\sigma_u$	−0.126645		−0.12664387(0)
$3\pi_u(4f)$		−0.12619892048	−0.12619892(1)
$1\delta_u$			−0.12496254(3)
$1\phi_u(4f)$		−0.123125506	−0.12312550(0)
$2\delta_g(4d)$		−0.1210194626	−0.12101946(3)
$4\pi_u$			−0.11591529(2)
$6\sigma_g$			−0.1054423(0)
$5\sigma_u$			−0.085938(9)
$7\sigma_g$			−0.08297(4)
$6\sigma_u$			−0.08084(4)
$3\pi_g(5d)$		−0.080833179	−0.08083(5)

[a] Ref 56. [b] Ref 58. [c] Ref 57. [d] Ref 40.

Table 6. Ground-State Total Energies and HOMO Energies, in hartree, for the He, Li, and Be Atoms, Calculated with xKLI and xOEP

	xKLI		xOEP	
atom	Grabo et al.[a]	DARSEC	Grabo et al.[a]	DARSEC
He	−2.8617	−2.8616(8)	−2.8617	−2.8616(8)
Li	−7.4324	−7.43243(5)	−7.4325	−7.4325(0)
Be	−14.5723	−14.57228(3)	−14.5724	−14.5724(3)

[a] Ref 11.

to previous work[59] (except for the $1\phi_u$, $2\delta_g$, and $3\pi_g$ orbitals, for which no such comparison was available).

As a second step in the evaluation of our all-electron xKLI and xOEP schemes, we compare calculations for polyelectron atoms with similar calculations performed on radial grids. Table 6 shows total energies of He, Li, and Be atoms, compared to the data of Grabo et al.[11] Selected eigenvalues for Li[60] and Be are given in Tables 7 and 8, respectively. In Table 7 the Li eigenvalues are compared to those obtained by Engel and Vosko,[37] as well as to independent calculations we performed using a 1D radial code.[14] In Table 8, the Be eigenvalues are compared to those obtained by Kümmel and Perdew.[14] Once again, an accuracy of 0.1 mhartree is achieved throughout. Furthermore, Tables 7 and 8 also

Table 7. Ground-State Energy Levels and $\Delta E_{x\sigma}^{\mathrm{vir}}$, in hartree, for the Li Atom, Calculated with xKLI and xOEP

	xKLI		xOEP		
Li	1D radial grid	DARSEC	1D radial grid	Engel and Vosko[a]	DARSEC
$1s\uparrow$	−2.08145	−2.0814(5)	−2.05453		−2.0545(3)
$2s\uparrow$	−0.19618	−0.1961(9)	−0.19629	−0.1963	−0.1962(8)
$\Delta E_{x\uparrow}^{\mathrm{vir}}$	0.00529	0.0053	1.28×10^{-7}	−0.000014	−0.00004
$1s\downarrow$	−2.46714	−2.4671(5)	−2.46884	−2.4688	−2.4688(5)
$2s\downarrow$		−0.3026(2)			−0.3031(3)
$\Delta E_{x\downarrow}^{\mathrm{vir}}$	10^{-10}	-3×10^{-7}	-2×10^{-9}	0.000004	−0.000009

[a] Ref 37.

Table 8. Ground-State Energy Levels and $\Delta E_x^{\mathrm{vir}}$, in hartree, for the Be Atom, Calculated with xKLI and xOEP

	xKLI		xOEP	
Be	1D radial grid[a]	DARSEC	1D radial grid[a]	DARSEC
1s	−4.1668	−4.1668(3)	−4.1257	−4.1257(1)
2s	−0.3089	−0.3088(5)	−0.3092	−0.3092(3)
$\Delta E_x^{\mathrm{vir}}$	∼1%	0.02 (0.78%)	0.00001,[b] $\sim 10^{-4}$%[a]	0.00001(4×10^{-4}%)

[a] Ref 14. [b] Ref 37.

Table 9. Ground-State Total Energy, Energy Levels, and $\Delta E_x^{\mathrm{vir}}$, in hartree, for LiH, Calculated with xKLI and xOEP

	xKLI		xOEP
LiH	Grabo et al.[a]	DARSEC	DARSEC
E_{tot}	−7.9868	−7.98680(8)	−7.98691(9)
1σ	−2.0786	−2.0786(0)	−2.069(4)
2σ	−0.3011	−0.3010(5)	−0.3015(9)
$\Delta E_x^{\mathrm{vir}}$		−0.02	−0.000098

[a] Ref 11.

Table 10. Ground-State Total Energy, Energy Levels, and $\Delta E_x^{\mathrm{vir}}$, in hartree, for BH, Calculated with xKLI and xOEP

	xKLI		xOEP
BH	Grabo et al.[a]	DARSEC	DARSEC
E_{tot}	−25.1290	−25.12903(0)	−25.12963(6)
1σ	−6.8624	−6.8623(6)	−6.8126(5)
2σ	−0.5856	−0.58561(5)	−0.577(4)
3σ	−0.3462	−0.34621(2)	−0.34729(7)
$\Delta E_x^{\mathrm{vir}}$		0.01	0.0003

[a] Ref 11.

provide the extent to which the exchange virial relation of Levy and Perdew[61]

$$E_{x,\sigma}[\rho(\mathbf{r})] = \int V_{x,\sigma}^{\mathrm{OEP}}(\mathbf{r})[3\rho_\sigma(\mathbf{r}) + \mathbf{r}\cdot\nabla\rho_\sigma(\mathbf{r})]\,\mathrm{d}^3 r \tag{17}$$

is obeyed, i.e., the difference between the left- and right-hand sides of the above equation, which is denoted by $\Delta E_{x\sigma}^{\mathrm{vir}}$. The resulting deviations are similar to those obtained in previous work[37,14] and, as expected, are significantly smaller for OEP than for KLI (except for the singly occupied spin down channel of Li in which the deviations are practically zero for both xKLI and xOEP).

We now turn to exact-exchange calculations of polyelectron diatomic molecules, starting with xKLI. Tables 9−11 provide total energies and energy levels for LiH, BH, and Li_2. These results are again compared to those of Grabo et al.,[11] where the same bond lengths were used. As with the single-atom systems, we find an agreement in the energies to the stated accuracy. Having verified our approach for a wide range of realistic scenarios, we can now turn to providing new fully numerical xOEP results for the total energy and energy levels of LiH, BH, and Li_2, using the same bond lengths that were used for the xKLI calculations. These results are given in Tables 9−11.

Table 11. Ground-State Total Energy, Energy Levels, and $\Delta E_x^{\mathrm{vir}}$, in hartree, for Li_2, Calculated with xKLI and xOEP

	xKLI		xOEP
Li_2	Grabo et al.[a]	DARSEC	DARSEC
E_{tot}	−14.8706	−14.87058(0)	−14.87076(5)
$1\sigma_g$	−2.0276	−2.0275(9)	−2.01(3)
$1\sigma_u$	−2.0272	−2.0272(4)	−2.01(3)
$2\sigma_g$	−0.1813	−0.1812(7)	−0.1818(3)
$\Delta E_x^{\mathrm{vir}}$		−0.04	−0.0000098

[a] Ref 11.

Although xOEP diatomic calculations that are not fully numerical certainly do exist,[5] we are not aware of independent fully numerical xOEP diatomic calculations to compare our results with.[62] In the absence of those, we confirm the correctness of our calculations by verifying that they satisfy several important criteria:[14] First, for the solution to be an OEP solution, it must satisfy eq 3, i.e., the function $S_\sigma(\mathbf{r})$ must vanish. With the xKLI potentials we find $|S_{\max}| \approx 10^{-2}$ a_0^{-3}, where a_0 is the atomic length unit, whereas for xOEP calculations converged to 10^{-4} hartree (in the total energy), $|S_{\max}|$ is typically of the order of 10^{-4} a_0^{-3} or less. Second, we verify that the obtained xOEP total energies are lower than the ones obtained by xKLI, i.e., $E_{\mathrm{tot}}^{\mathrm{xOEP}} \le E_{\mathrm{tot}}^{\mathrm{xKLI}}$. This must be the case as the OEP solution rigorously satisfies a variational principle minimization, whereas the xKLI solution does not.[63] Third, a lower bound for the xOEP total energy is provided by the HF total energy, i.e., $E_{\mathrm{tot}}^{\mathrm{HF}} \le E_{\mathrm{tot}}^{\mathrm{xOEP}}$. This is because the xOEP potential must be a local one, whereas the HF potential has no such constraint.[63] We verified that our xOEP total energies indeed satisfy this relation by comparing them to the following HF total energies, obtained by Laaksonen et al.[40] from fully numerical calculations conducted using a similar prolate-spheroidal grid and the same bond lengths: $E_{\mathrm{LiH}}^{\mathrm{HF}} = -7.9874$, $E_{\mathrm{BH}}^{\mathrm{HF}} = -25.1316$, $E_{\mathrm{Li_2}}^{\mathrm{HF}} = -14.8716$. These HF energies are all lower than the corresponding xOEP total energies. The xOEP total energies of atoms are closer to the corresponding xKLI total energies than to the HF total energies.[11] This behavior was also observed here for the diatomic calculations. Fourth, we calculated the value of $\Delta E_{x\sigma}^{\mathrm{vir}}$ to make sure that the virial exchange relation of eq 17 holds. We find that, whereas it is slightly violated by the KLI approximation, with an error in the order of 0.01 hartree, with OEP calculations converged to 10^{-4} hartree in the total energy, the virial exchange relation is also typically satisfied to $\sim 10^{-4}$ hartree or better. Last, according to available atomic xOEP calculations[11,14,37,50] the xOEP solutions for the highest occupied eigenvalue are lower than those of xKLI. This is reasonable, because OEP leads to stronger binding than KLI.[11] This results in a higher ionization potential, which equals the negative of the highest

occupied eigenvalue in exact Kohn−Sham theory.[64,65] Tables 9−11 confirm that this trend is also found here.

We end this section with our representative case of the CO molecule. Whereas with xKLI we got a total energy of −112.7832 hartree, the xOEP total energy turns out to be −112.785(3) hartrees. Interestingly, a previously reported OEP calculation for CO performed using basis sets[66] yielded a total energy of −112.77652 hartree. This value is higher than the corresponding KLI one, as also pointed out by Engel et al.[43] This underscores the importance of fully numerical all-electron OEP calculations. In calculations that are not fully numerical, even when the computation is numerically converged it may still contain errors that are inherent in the approximations made.

4. Conclusions

We presented an approach for fully numerical, all-electron solutions of the OEP equation within Kohn−Sham DFT for diatomic molecules. The approach is based on a real-space, prolate-spheroidal coordinate grid for solving the all-electron Kohn−Sham equations and an iterative scheme for solving the OEP equation. The accuracy of the approach, as implemented by us in the DARSEC program, was demonstrated by comparison with previously reported results within LDA, xKLI, and xOEP calculations. Finally, new benchmark fully numerical xOEP results for selected diatomic molecules were provided. Because our method is free of any approximation other than the choice of the approximate exchange-correlation energy functional (and unavoidable numerical roundoff errors), we believe that it may serve as a powerful tool for systematic testing and evaluation of orbital-dependent functionals.

Acknowledgment. This work was supported by the Minerva Foundation, the Minerva−Schmidt Center for Supra-Molecular Chemistry, the Lise Meitner−Minerva Center for Computational Quantum Chemistry, and the German−Israeli Foundation. A.M. thanks Dubi Kelmer for many illuminating discussions and Amir Natan for much help.

Appendix A: Non-Hermiticity of the Laplacian

In the prolate-spheroidal coordinate system, the Laplacian operator, Δ_m of eq 9, is not Hermitian (with respect to a standard inner product). This is because it is a weighted sum of second derivatives, which are Hermitian operators, and first derivatives, which are anti-Hermitian operators. This raises additional numerical issues, which are discussed in this Appendix. We show that although the problem may be completely resolved analytically, it reappears upon discretization of the Kohn−Sham equation. The discretization then either approximates the analytical operator extremely well, but is only almost Hermitian (i.e., most, but not all, of its entries, obey Hermiticity), or it yields a strictly Hermitian matrix, but may be an insufficiently accurate approximation to the analytical operator.

For any differential operator that is Hermitian in Cartesian coordinates but is not Hermitian in some other coordinate system, it is always possible to regain Hermiticity by multiplying with the corresponding Jacobian, $\mathcal{J}$. In particular, for the Laplacian operator in prolate-spheroidal coordinates, we have

Table A1. Ground-State Energy Levels, in rydberg, for the H Atom, Calculated with xKLI Using Non-Hermitian (Third Column) and Hermitian (Fourth Column) Hamiltonians[a]

H	exact	$\mathbf{D}_\alpha^m\mathbf{G}_\alpha\mathbf{D}_\alpha^m$	$-(\mathbf{D}_\alpha^m)^{\mathrm{T}}\mathbf{G}_\alpha\mathbf{D}_\alpha^m$
1s	−1	−1.0000000	−1.00065
2s	−1/4	−0.2500000	−0.25053
2p	−1/4	−0.2500000	−0.25007
	−1/4	−0.2500000	−0.24986
	−1/4	−0.2500000	−0.24986

[a] An expansion order of $2L = 12$ neighbors was used.

$$\int f^*(\mathcal{J}\Delta_m g)\,d\mu\,d\nu\,d\phi = \int f^*(\nabla^2 g)\,dx\,dy\,dz = \int (\nabla^2 f)^* g\,dx\,dy\,dz = \int (\mathcal{J}\Delta_m f)^* g\,d\mu\,d\nu\,d\phi \quad \text{(A1)}$$

where the Jacobian, $\mathcal{J}(\mu, \nu, \phi)$, is a real function, given by eq 16. Multiplying both sides of the Kohn−Sham eq 1 by the Jacobian yields

$$\mathcal{J}\left(-\frac{1}{2}\Delta_m + V_{\mathrm{KS}}\right)\varphi_i = \varepsilon_i \mathcal{J}\varphi_i \quad \text{(A2)}$$

where some algebraic manipulation shows that the operator $\mathcal{J}\Delta_m$ is given by

$$\mathcal{J}\Delta_m(\mu,\nu) = \frac{R}{2}\left[\sin(\nu)\left(\frac{\partial}{\partial\mu}\sinh(\mu)\frac{\partial}{\partial\mu}\right) + \sinh(\mu)\left(\frac{\partial}{\partial\nu}\sin(\nu)\frac{\partial}{\partial\nu}\right) - m^2\left(\frac{\sin(\nu)}{\sinh(\mu)} + \frac{\sinh(\mu)}{\sin(\nu)}\right)\right] \quad \text{(A3)}$$

In this formulation, the Kohn−Sham Hamiltonian is rigorously Hermitian, at the cost of having to solve a generalized eigenvalue problem.

We now consider the discrete representation of eq A3. Clearly, the operator $\mathcal{J}\Delta_m$ is Hermitian in its discrete matrix form if and only if the operator $((\partial/\partial\alpha)g_\alpha(\alpha)(\partial/\partial\alpha))$, where $\alpha = \mu, \nu$ and $g_\alpha =$ sinh, sin, respectively, is represented by a Hermitian matrix. We denote the matrix representation for the usual high-order finite difference expansion of a first partial derivative $\partial/\partial\alpha$ by a matrix $\mathbf{D}_\alpha$. The function g_α is represented by the appropriate diagonal matrix $\mathbf{G}_\alpha$. Normally, the complete operator $((\partial/\partial\alpha)g_\alpha(\alpha)(\partial/\partial\alpha))$ can then be represented as either $[\mathbf{D}_\alpha\mathbf{G}_\alpha\mathbf{D}_\alpha]$ or $[-\mathbf{D}_\alpha^{\mathrm{T}}\mathbf{G}_\alpha\mathbf{D}_\alpha]$. The latter expression is manifestly Hermitian, but normally so is the former because $\mathbf{D}_\alpha$ is anti-Hermitian, i.e., $\mathbf{D}_\alpha^{\mathrm{T}} = -\mathbf{D}_\alpha$. Unfortunately, here the matrix representation of $\mathbf{D}_\alpha$ is complicated by the boundary conditions: If a grid point is near the boundary, values of neighbors lying beyond the boundary (i.e., across the $\mu = 0$, $\nu = 0$, or $\nu = \pi$ lines, or, equivalently, across the interatomic axis in real space) need to be taken into account for evaluating the derivative in that point. These are taken as plus or minus the values at the mirror positions inside the boundary, depending on the angular momentum number m, which dictates the parity of the wave function.[41] Formally, the $2L$th order finite difference matrix representation of the first derivative, for a function with angular number m, then assumes the following form (given here for derivation along μ as an example)

$$\mathbf{D}_{\mu}^{m}(i,j)=\begin{cases}0 & i_\nu \neq j_\nu \text{ or } |i_\mu - j_\mu| > L \\ C_{j_\mu - i_\mu} & i_\nu = j_\nu \text{ and } |i_\mu - j_\mu| \leq L \\ & \quad \text{and } i_\mu - (-j_\mu) > L \\ C_{j_\mu - i_\mu} + (-1)^m C_{-j_\mu - i_\mu} & i_\nu = j_\nu \text{ and } |i_\mu - j_\mu| \leq L \\ & \quad \text{and } i_\mu - (-j_\mu) \leq L \end{cases} \tag{A4}$$

Here, i, j are running indices of two arbitrary grid points and i_α, j_α are running indices for the same two points along the one-dimensional direction α.[67] The weight of the kth neighbor for the first derivative in the high-order finite difference scheme is given by C_k.[44] Because $C_{-k} = -C_k$, it follow that $\mathbf{D}_{\alpha}^{m}(i,j) = -\mathbf{D}_{\alpha}^{m}(j,i)$ for most i,j entries. However, for i, j pairs that are near the boundaries, i.e., belonging in the last line of eq A4, $\mathbf{D}_{\alpha}^{m}(i,j) \neq -\mathbf{D}_{\alpha}^{m}(j,i)$, and consequently $\mathbf{D}_{\alpha}^{m}$ is neither Hermitian nor anti-Hermitian. Thus, the representations $[\mathbf{D}_{\alpha}^{m}\mathbf{G}_{\alpha}\mathbf{D}_{\alpha}^{m}]$ and $[-(\mathbf{D}_{\alpha}^{m})^{\mathrm{T}}\mathbf{G}_{\alpha}\mathbf{D}_{\alpha}^{m}]$ are not equivalent, and only the latter must be Hermitian.

Careful consideration of the structure of the matrix $\mathbf{D}_{\alpha}^{m}$ of eq A4 reveals that $[\mathbf{D}_{\alpha}^{m}]^{\mathrm{T}} = -\mathbf{D}_{\alpha}^{m+1}$. Therefore, $[-(\mathbf{D}_{\alpha}^{m})^{\mathrm{T}}\mathbf{G}_{\alpha}\mathbf{D}_{\alpha}^{m}] = [\mathbf{D}_{\alpha}^{m+1}\mathbf{G}_{\alpha}\mathbf{D}_{\alpha}^{m}]$ differs from $[\mathbf{D}_{\alpha}^{m}\mathbf{G}_{\alpha}\mathbf{D}_{\alpha}^{m}]$ solely in the parity of the left-most matrix. Unfortunately, parity considerations show that it is the latter, non-Hermitian form, rather than the former, Hermitian form, which is the correct one. Importantly, this undesirable tradeoff between accuracy and Hermiticity of the representation is a direct consequence of using a high-order expansion. For $L = 1$, i.e., use of immediate neighbors only (and with the interatomic axis explicitly used), the problem does not arise. However, this clearly comes at the cost of a significant reduction in numerical accuracy, per a given grid step.

The numerical consequences of the difference between the two representation schemes are illustrated in Table A1. For a single H atom, it compares the known analytical results to those of xKLI calculations, diagonalized with the above two matrix representations (and all else being equal). Clearly, the "almost Hermitian" representation (third column) yields results that are accurate to all digits shown, whereas the Hermitian representation (fourth column) produces relatively poor results.

A different perspective on the above considerations can be obtained from variational arguments. Equation A2 can also be derived from the variational principle: Let F be a functional given by

$$\mathrm{F} = \underbrace{\frac{1}{2}\int |\nabla\varphi_i(\mathbf{r})|^2 d^3r}_{\mathrm{T}} + \underbrace{\int (V_{KS}(\mathbf{r}) - \varepsilon_i)|\varphi_i(\mathbf{r})|^2 d^3r}_{\mathrm{I}} ,$$

$$\frac{\delta \mathrm{F}}{\delta\varphi_i(\mathbf{r})} = 0 \quad \forall \mathbf{r}, \tag{A5}$$

then setting the variation of F with respect to $\varphi_i(\mathbf{r})$ to zero, where all variation is performed in the prolate-spheroidal coordinate system, yields eq A2.

Becke suggested that a discrete prolate-spheroidal Hermitian representation for the Kohn−Sham equations can be obtained by discretizing the functional of eq A5 and performing the variation on the discrete form.[39] The discrete variation leads to the Hermitian representation, $-[(\mathbf{D}_{\alpha}^{m})^{\mathrm{T}}\mathbf{G}_{\alpha}\mathbf{D}_{\alpha}^{m}]$,[39] obtained above from a different set of considerations. This means that we have obtained an insufficiently accurate representation despite starting from a completely equivalent analytical expression, a result which merits an explanation. A key issue in this respect is that in the functional F of eq A5, the kinetic energy term is expressed as $(1/2)\int|\nabla\varphi_i(\mathbf{r})|^2\ \mathrm{d}^3r$ and not as $-(1/2)\int\varphi_i^*(\mathbf{r})\nabla^2\varphi_i(\mathbf{r})\ \mathrm{d}^3r$. Normally, the two expression are equivalent analytically by virtue of Green's first identity. But numerically, because of the "mirror" or "antimirror" boundary conditions imposed by the prolate-spheroidal coordinate system, Green's identity is no longer obeyed after discretization. To see that, consider that in prolate-spheroidal coordinates, use of the alternative definition for the kinetic energy, $(1/2)\int|\nabla\varphi_i(\mathbf{r})|^2\ \mathrm{d}^3r$, would lead to one-dimensional integrals, and therefore discretization, of the type

$$\int \left(\frac{\partial}{\partial\alpha}\varphi_i(\mu,\nu,\phi)\right)^*\left(\frac{\partial}{\partial\alpha}\varphi_i(\mu,\nu,\phi)\right)g_\alpha(\alpha)\,\mathrm{d}\alpha \Rightarrow$$
$$\langle\mathbf{D}_{\alpha}^{m}\varphi_i|\mathbf{G}_{\alpha}\mathbf{D}_{\alpha}^{m}\varphi_i\rangle = \langle\varphi_i|(\mathbf{D}_{\alpha}^{m})^{\mathrm{T}}\mathbf{G}_{\alpha}\mathbf{D}_{\alpha}^{m}\varphi_i\rangle \quad \alpha = \mu,\nu \tag{A6}$$

However, the original definition for the kinetic energy, $-(1/2)\int\varphi_i^*(\mathbf{r})\nabla^2\varphi_i(\mathbf{r})\ \mathrm{d}^3r$, leads to different one-dimensional integrals, and hence discretization

$$-\int\varphi_i^*(\mu,\nu,\phi)\left(\frac{\partial}{\partial\alpha}g_\alpha(\alpha)\frac{\partial}{\partial\alpha}\right)\varphi_i(\mu,\nu,\phi)\,\mathrm{d}\alpha \Rightarrow$$
$$-\langle\varphi_i|\mathbf{D}_{\alpha}^{m}\mathbf{G}_{\alpha}\mathbf{D}_{\alpha}^{m}\varphi_i\rangle, \qquad \alpha = \mu,\nu \tag{A7}$$

As explained above, the two forms would have been equivalent had $(\mathbf{D}_{\alpha}^{m})^{\mathrm{T}} = -\mathbf{D}_{\alpha}^{m}$, but as this is not the case, only the latter, non-Hermitian form, is accurate.

Appendix B: Computing the Orbital Shifts

The OEP method requires the construction of "orbital shifts", $\psi_{i\sigma}(\mathbf{r})$, defined in eq 4. According to this equation, $\psi_{i\sigma}(\mathbf{r})$ may be interpreted as the negative of the first-order orbital correction that results if a Kohn−Sham orbital, $\varphi_{i\sigma}(\mathbf{r})$, is subjected to the perturbation[15]

$$\Delta v_{i\sigma}(\mathbf{r}) = u_{i\sigma}(\mathbf{r}) - V_{\mathrm{xc},\sigma}^{\mathrm{OEP}}(\mathbf{r}) \tag{B1}$$

The orbital shifts may thus be computed using first-order perturbation theory from

$$(H_{\mathrm{KS}} - \varepsilon_{i\sigma}^{0})\psi_{i\sigma}(\mathbf{r}) = -(\varepsilon_{i\sigma}^{1} - \Delta v_{i\sigma}(\mathbf{r}))\varphi_{i\sigma}(\mathbf{r}) \tag{B2}$$

where $\varepsilon_{i\sigma}^{0}$ is the ith Kohn−Sham eigenvalue and $\varepsilon_{i\sigma}^{1}$ is its first-order correction.[10,50] The solution of eq B2 is obtained numerically by using the conjugate gradient (CG)[49] method. In practice, solving this equation in DARSEC with the prolate-spheroidal coordinates requires several observations:

First, following eq 4 and using the rotational symmetry of the perturbed potential, $\Delta v_{i\sigma}(\mu,\nu,\phi) = \Delta v_{i\sigma}(\mu,\nu,0)$, the orbital shifts can be shown to have the same rotational symmetry as their associated Kohn−Sham orbitals

$$\varphi_{k\sigma}(\mu,\nu,\phi) = \varphi_{k\sigma}(\mu,\nu,0)\mathrm{e}^{\mathrm{i}m_k\phi} \Leftrightarrow \psi_{k\sigma}(\mu,\nu,\phi) = \psi_{k\sigma}(\mu,\nu,0)\mathrm{e}^{\mathrm{i}m_k\phi} \tag{B3}$$

Second, the CG method assumes Hermiticity of the inverted operator, whereas in DARSEC the Kohn−Sham matrix is not Hermitian (see Appendix A). This difficulty is present in all other CG applications in DARSEC, but it is usually solved by multiplying both sides of the equation by the volume element $\mathcal{J}(\mu, \nu, \phi)$ (eq 16), which makes the matrix Hermitian "enough" for the CG method to work properly. In the case of eq B2, however, the non-Hermiticity of the matrix is more severe as it also influences the evaluation of the $\varepsilon^1_{i\sigma}$ term in eq B2. This is because the usual expression, given by $\varepsilon^1_{i\sigma} = \langle\varphi_{i\sigma}|\Delta v_{i\sigma}|\varphi_{i\sigma}\rangle \equiv \overline{\Delta v_{i\sigma}(\mathbf{r})}$ is no longer valid. Instead, first-order perturbation theory for a general (not necessarily Hermitian) operator shows that $\varepsilon^1_{i\sigma}$ generally takes the following form

$$\varepsilon^1_{i\sigma} = \langle\varphi_{i\sigma}|\Delta v_{i\sigma}|\varphi_{i\sigma}\rangle + \langle\psi_{i\sigma}|H_{\mathrm{KS}}|\varphi_{i\sigma}\rangle + \langle\varphi_{i\sigma}|H_{\mathrm{KS}}|\psi_{i\sigma}\rangle \tag{B4}$$

For a Hermitian operator, eq B4 properly reduces to the usual expression due to the orthogonality between $\varphi_{i\sigma}(\mathbf{r})$ and its orbital shift, $\psi_{i\sigma}(\mathbf{r})$.[14] Since the Kohn−Sham Hamiltonian in DARSEC is represented by an almost Hermitian matrix, the resulting orbitals are no longer fully orthogonal and the matrix cannot be applied to the left. As a result, all the terms of eq B4 must be taken explicitly into account when eq B2 is solved. To make this equation compatible with the required CG form—a known matrix **A** on the left-hand side and a known vector **b** on the right-hand side—we rearrange it in the form

$$\underbrace{\left[H_{KS} - \varepsilon^0_{i\sigma} - \varepsilon^0_{i\sigma}|\varphi_{i\sigma}\rangle\langle\varphi_{i\sigma}| - |\varphi_{i\sigma}\rangle\langle\varphi_{i\sigma}|H_{KS}\right]}_{A} \underbrace{|\psi_{i\sigma}\rangle}_{x} = \underbrace{-(\overline{\Delta v_{i\sigma}(\mathbf{r})} - \Delta v_{i\sigma}(\mathbf{r}))|\varphi_{i\sigma}\rangle}_{b} \tag{B5}$$

Because the deviation from Hermiticity of the Hamiltonian matrix is relatively small (see Appendix A), the added terms $\langle\psi_{i\sigma}|H_{\mathrm{KS}}|\varphi_{i\sigma}\rangle$ and $\langle\varphi_{i\sigma}|H_{\mathrm{KS}}|\psi_{i\sigma}\rangle$ are also small, of the order of 10^{-4} hartree. Still, including them in the calculations was found to be crucial for getting converged solutions.

Third, we have found it numerically useful to compute the orbital shifts in two successive steps: At first, we find an approximation to the orbital shifts by solving eq B2 with $\varepsilon^1_{i\sigma} = \overline{\Delta v_{i\sigma}(\mathbf{r})}$, using the symmetric (but inaccurate) Hamiltonian matrix. In the second and final step the CG method is applied once again, but now it solves eq B5 with the highly accurate (almost symmetric) Hamiltonian matrix and with the previously found orbital shift approximations as initial guess vectors.

References

(1) Hohenberg, P.; Kohn, W. *Phys. Rev. B* **1964**, *136*, 864.

(2) Kohn, W.; Sham, L. J. *Phys. Rev. A* **1965**, *140*, 1133.

(3) Dreizler, R. M.; Gross, E. K. U. *Density Functional Theory: An Approach to the Quantum Many-Body Problem*; Springer: Berlin, 1990.

(4) von Barth, U.; Hedin, L. *J. Phys. C* **1972**, *5*, 1629.

(5) Kümmel, S.; Kronik, L. *Rev. Mod. Phys.* **2008**, *80*, 3.

(6) Sharp, R. T.; Horton, G. K. *Phys. Rev.* **1953**, *90*, 317.

(7) Talman, J. D.; Shadwick, W. F. *Phys. Rev. A* **1976**, *14*, 36.

(8) Görling, A.; Levy, M. *Phys. Rev. A* **1994**, *50*, 196.

(9) Görling, A.; Levy, M. *Int. J. Quantum Chem. Symp.* **1995**, *29*, 93.

(10) Grabo, T.; Kreibich, T.; Gross, E. K. U. *Mol. Eng.* **1997**, *7*, 27.

(11) Grabo, T.; Kreibich, T.; Kurth, S.; Gross, E. K. U. In *Strong Coulomb Correlation in Electronic Structure: Beyond the Local Density Approximation*; Anisimov, V. I. , Ed.; Gordon & Breach: Amsterdam, The Netherlands, 2000; pp 203−317.

(12) Görling, A. *J. Chem. Phys.* **2005**, *123*, 062203.

(13) Krieger, J. B.; Li, Y.; Iafrate, G. J. *Phys. Rev. A* **1992**, *46*, 5453.

(14) Kümmel, S.; Perdew, J. P. *Phys. Rev. B* **2003**, *68*, 035103.

(15) Krieger, J. B.; Li, Y.; Iafrate, G. J. *Phys. Rev. A* **1992**, *45*, 101.

(16) Gritsenko, O. V.; Baerends, E. J. *Phys. Rev. A* **2001**, *64*, 042506.

(17) Della Sala, F.; Görling, A. *J. Chem. Phys.* **2001**, *115*, 5718.

(18) Wilson, P. J.; Tozer, D. J. *Chem. Phys. Lett.* **2001**, *337*, 341.

(19) Arbuznikov, A. V.; Kaupp, M. *Chem. Phys. Lett.* **2004**, *386*, 8.

(20) Kümmel, S.; Kronik, L.; Perdew, J. P. *Phys. Rev. Lett.* **2004**, *93*, 213002.

(21) Rinke, P.; Qteish, A.; Neugebauer, J.; Scheffler, M. *Phys. Status Solidi B* **2008**, *245*, 929.

(22) Körzdörfer, T.; Mundt, M.; Kümmel, S. *Phys. Rev. Lett.* **2008**, *100*, 133004.

(23) Körzdörfer, T.; Kümmel, S.; Mundt, M. *J. Chem. Phys.* **2008**, *129*, 014110.

(24) Bylander, D. M.; Kleinman, L. *Phys. Rev. B* **1995**, *52*, 14566.

(25) Städele, M.; Moukara, M.; Majewski, J. A.; Vogl, P.; Görling, A. *Phys. Rev. B* **1999**, *59*, 10031.

(26) Moukara, M.; Städele, M.; Majewski, J. A.; Vogl, P.; Görling, A. *J. Phys.: Condens. Matter* **2000**, *12*, 6783.

(27) Engel, E.; Höck, A.; Schmid, R. N.; Dreizler, R. M.; Chetty, N. *Phys. Rev. B* **2001**, *64*, 125111.

(28) Sharma, S.; Dewhurts, J. K.; Ambrosch-Draxl, C. *Phys. Rev. Lett.* **2005**, *95*, 136402.

(29) Hirata, S.; Ivanov, S.; Grabowski, I.; Bartlett, R. J.; Burke, K.; Talman, J. D. *J. Chem. Phys.* **2001**, *115*, 1635.

(30) Staroverov, V. N.; Scuseria, G. E.; Davidson, E. R. *J. Chem. Phys.* **2006**, *124*, 141103.

(31) Staroverov, V. N.; Scuseria, G. E.; Davidson, E. R. *J. Chem. Phys.* **2006**, *125*, 081104.

(32) Izmaylov, A. F.; Staroverov, V. N.; Scuseria, G. E.; Davidson, E. R.; Stoltz, G.; Cancès, E. *J. Chem. Phys.* **2007**, *126*, 084107.

(33) Hesselmann, A.; Götz, A. W.; Della Sala, F.; Görling, A. *J. Chem. Phys.* **2007**, *127*, 054102.

(34) Heaton-Burgess, T.; Bulat, F. A.; Yang, W. *Phys. Rev. Lett.* **2007**, *98*, 256401.

(35) Görling, A.; Hesselmann, A.; Jones, M.; Levy, M. *J. Chem. Phys.* **2008**, *128*, 104104.

(36) Heaton-Burgess, T.; Yang, W. *J. Chem. Phys.* **2008**, *129*, 194102.

(37) Engel, E.; Vosko, S. H. *Phys. Rev. A* **1993**, *47*, 2800.

(38) Gálvez, F. J.; Buendía, E.; Maldonado, P.; Sarsa, A. J. *Eur. Phys. J. D* **2008**, *50*, 229–235.

(39) Becke, A. D. *J. Chem. Phys.* **1982**, *76*, 6037.

(40) Laaksonen, L.; Pyykkö, P.; Sundholm, D. *Comp. Phys. Rep.* **1986**, *4*, 313.

(41) Kobus, J.; Laaksonen, L.; Sundholm, D. *Comput. Phys. Commun.* **1996**, *98*, 346.

(42) Engel, E.; Höck, A.; Dreizler, R. M. *Phys. Rev. A* **2000**, *61*, 032502.

(43) Engel, E.; Höck, A.; Dreizler, R. M. *Phys. Rev. A* **2000**, *62*, 042502.

(44) Fornberg, B. *Math. Comput.* **1988**, *51*, 699.

(45) Beck, T. L. *Rev. Mod. Phys.* **2000**, *72*, 1041.

(46) (a) Chelikowsky, J. R.; Troullier, N.; Saad, Y. *Phys. Rev. Lett.* **1994**, *72*, 1240. (b) Chelikowsky, J. R.; Troullier, N.; Wu, K.; Saad, Y. *Phys. Rev. B* **1994**, *50*, 11355.

(47) Chelikowsky, J. R. *J. Phys. D* **2000**, *33*, R33.

(48) Kronik, L.; Makmal, A.; Tiago, M. L.; Alemany, M. M. G.; Jain, M.; Huang, X.; Saad, Y.; Chelikowsky, J. R. *Phys. Status Solidi B* **2006**, *243*, 1063.

(49) Reid, J. K. In *Large Sparse Sets of Linear Equations: Proceedings of the Oxford Conference of the Institute of Mathematics and Its Applications*; Reid, J. K. Ed.; Academic Press: London, United Kingdom, 1971; pp 231−254.

(50) Kümmel, S.; Perdew, J. P. *Phys. Rev. Lett.* **2003**, *90*, 043004.

(51) (a) Define $p(i) = ((i-1) \text{ modulo } 6) + 1$. Then $\tilde{c}_i = c_{p(i)}$ except at points which are the upper end of one seven-point integration and the lower end of another, at which $\tilde{c}_i = 2c_{p(i)}$. (b) When the interatomic axis is avoided by shifting the grid points by half-step size (second grid type) we use the "trapezoid rule" to allow for integration up to the interatomic axis. Consequently, the values of $\tilde{c}_{\mu_1}$, $\tilde{c}_{\nu_1}$, and $\tilde{c}_{\nu_{N_\nu}}$ are increased by 1/4 (note that the volume element $\mathcal{J}(\mu, \nu, \phi)$ vanishes at this axis).

(52) Lehoucq, R. B.; Maschhoff, K.; Sorensen, D.; Yang, C. ARPACK-Arnoldi Package. http://www.caam.rice.edu/software/ARPACK/ (accessed Apr 23, 2009).

(53) Carbon monoxide NIST. http://webbook.nist.gov/cgi/cbook.cgi?Formula=CO&NoIon=on&Units=SI&cDI=on (accessed Apr 23, 2009).

(54) Ceperley, D. M.; Alder, B. J. *Phys. Rev. Lett.* **1980**, *45*, 566.

(55) Perdew, J. P.; Wang, Y. *Phys. Rev. B* **1992**, *45*, 13244.

(56) Bates, D. R.; Ledsham, K.; Stewart, A. L. *Philos. Trans. R. Soc. London, Ser. A* **1953**, *246*, 215.

(57) Wind, H. *J. Chem. Phys.* **1965**, *42*, 2371.

(58) Laaksonen, L.; Pyykkö, P.; Sundholm, D. *Int. J. Quantum Chem.* **1983**, *23*, 309.

(59) Madsen, M. M.; Peek, J. M. *At. Data* **1971**, *2*, 171.

(60) The results for Li, in our work as well as in previous studies, violate the aufbau principle, i.e., the energy levels are not occupied in ascending order. This is clearly seen in Table 7, where the second state of the spin down channel is not occupied even though its eigenvalue is lower than the eigenvalue of the occupied second state of the spin up channel. We interpret this as a failure of the exchange-only approximation and an indicator of the qualitative importance of correlation in the electronic structure of Li.

(61) Levy, M.; Perdew, J. P. *Phys. Rev. A* **1985**, *32*, 2010.

(62) Note that our fully numerical results for the total energy of LiH do agree well with the results obtained using Gaussian basis sets (ref 17).

(63) Krieger, J. B.; Li, Y.; Iafrate, G. J. In *Density Functional Theory*; Gross, E. K. U., Dreizler, R. M. , Eds.; Plenum Press: New York, 1995; p 191.

(64) Levy, M.; Perdew, J. P.; Sahni, V. *Phys. Rev. A* **1984**, *30*, 2745.

(65) Almbladh, C.-O.; von Barth, U. *Phys. Rev. B* **1985**, *31*, 3231.

(66) Ivanov, S.; Hirata, S.; Bartlett, R. J. *Phys. Rev. Lett.* **1999**, *83*, 5455.

(67) (a) The analogous expression for the ν derivative must also consider the boundary at $\nu = \pi$:

$$\mathbf{D}^m_\nu(i,j) = \begin{cases} 0 & i_\mu \neq j_\mu \text{ or } |i_\nu - j_\nu| > L \\ C_{j_\nu - i_\nu} & i_\mu = j_\mu \text{ and } |i_\nu - j_\nu| \leq L \\ & \quad \text{and } (i_\nu - (-j_\nu)) > L \\ & \quad \text{and } 2N_\nu - i_\nu - j_\nu > L) \\ C_{j_\nu - i_\nu} + (-1)^m C_{-j_\nu - i_\nu} & i_\mu = j_\mu \text{ and } |i_\nu - j_\nu| \leq L \\ & \quad \text{and } i_\nu - (-j_\nu) \leq L \\ C_{j_\nu - i_\nu} + (-1)^m C_{2N_\nu - j_\nu - i_\nu + 2} & i_\mu = j_\mu \text{ and } |i_\nu - j_\nu| \leq L \\ & \quad \text{and } 2N_\nu - j_\nu - i_\nu + 2 \leq L \end{cases}$$

(b) This description is suitable for grids that use the interatomic axis. For the second grid type in which the interatomic axis is avoided, entries near the boundaries are given by $C_{j_\alpha - i_\alpha} + (-1)^m C_{-i_\alpha - j_\alpha + 1}$ for $-i_\alpha - j_\alpha + 1 \leq L$ (and for the $\nu = \pi$ boundary: $C_{j_\nu - i_\nu} + (-1)^m C_{2N_\nu - i_\nu - j_\nu + 1}$ for $2N_\nu - i_\nu - j_\nu + 1 \leq L$).

CT800485V